

**Rupa Sarkar**  
**Samir Kumar Pal**  
Department of Chemical,  
Biological and  
Macromolecular Sciences,  
Unit for Nano  
Science and Technology,  
S. N. Bose National  
Centre for Basic Sciences,  
Block JD, Sector III,  
Salt Lake,  
Kolkata 700 098, India

---

# Ligand–DNA Interaction in a Nanocage of Reverse Micelle

Received 20 May 2006;  
revised 14 September 2006;  
accepted 14 September 2006

Published online 18 September 2006 in Wiley InterScience (www.interscience.wiley.com). DOI 10.1002/bip.20606

**Abstract:** We have studied intercalation of ethidium bromide (EB) to genomic DNA encapsulated in a nanospace of an anionic AOT reverse micelle (RM). Circular dichroism (CD) study on the DNA in the RM reveals its condensed form. Here, we have used temporal decay-associated spectra (DAS) and time-resolved area normalized emission spectral (TRANES) techniques to investigate EB-binding to condensed DNA because the interference of emission from unbound EB in the RM makes conventional steady state and picosecond resolved fluorescence spectroscopic techniques challenging. The binding affinity of the ligand EB with the DNA in the RM is found to increase with the size of the RM, reflecting the effect of lessening of DNA condensation on the binding affinity. CD spectra of the DNA in the RM with various sizes indicate the structural change of the condensed DNA with reverse micellar size. DAS and TRANES techniques along with dynamic light scattering studies of the EB-DNA complex in the RM further reveal two kinds of binding modes of the ligand with the condensed DNA even in essentially monodispersed RMs. To investigate the role of RM on the ligand binding and secondary structure of the DNA, we have also studied complexation of EB with two synthetic self-complementary oligonucleotides of sequences (CGCAAATTTGCG)<sub>2</sub> and (CGCGCGCGCGCG)<sub>2</sub> in the RM. © 2006 Wiley Periodicals, Inc. *Biopolymers* 83: 675–686, 2006

This article was originally published online as an accepted preprint. The “Published Online” date corresponds to the preprint version. You can request a copy of the preprint by emailing the *Biopolymers* editorial office at [biopolymers@wiley.com](mailto:biopolymers@wiley.com)

**Keywords:** molecular recognition; intercalation; nanocage; base pair stacking; ligand binding; DNA condensation

---

## INTRODUCTION

The molecular recognition of DNA by small ligand molecules is important for the design of novel pharmaceuticals.<sup>1</sup> As the common conformation of DNA in a physiological condition is in a condensed form (e.g.

chromatin), the mechanism of molecular recognition must get addressed in the compact form of DNA. A number of condensing agents including neutral and anionic polymers and salts were reported to demonstrate the condensation of DNA in vitro.<sup>2–6</sup> Encapsulation of DNA in anionic AOT (bis(2-ethylhexyl)sul-

---

Correspondence to: Samir Kumar Pal; e-mail: [skpal@bose.res.in](mailto:skpal@bose.res.in)

Contract grant sponsor: DST  
Contract grant number: SR/FTP/PS-05/2004.

*Biopolymers*, Vol. 83, 675–686 (2006)

© 2006 Wiley Periodicals, Inc.



fosuccinate) reverse micelles (RM) is also found to be an efficient and convenient technique for the condensation of oligomolecular form of DNA molecule in the solution phase.<sup>7–10</sup> In one of these studies,<sup>10</sup> hybridization of a DNA in the RM was investigated and found to be retarded significantly when compared with that in bulk buffer. In a recent study from our group<sup>11</sup> by using steady-state and time resolved fluorescence energy transfer technique, we show that the compactness of the DNA in the RM depends on the degree of hydration.

In the present study we use a DNA intercalator ethidium bromide (EB) as a probe ligand. EB is known since a long time as a very convenient probe of DNA structure,<sup>12,13</sup> particularly a tool for determining the structure of DNA inside chromatin.<sup>14–17</sup> One of the early studies<sup>14</sup> confirmed the presence of high affinity EB-binding sites in the chromatin but not in the core particle, i.e. when linker is removed. The study also showed two types of EB-binding sites, namely, high affinity and cooperative, in the core particles. In this study, our major focus is to explore the nature of EB-binding to synthetic and genomic DNA upon encapsulation in anionic AOT RM. To investigate the structural change of genomic and synthetic DNA, we have used circular dichroism (CD) spectroscopy, and confirmed that genomic DNA in the nanocage of RM assumes condensed form, which is consistent with other reports.<sup>18,19</sup> Dynamic light scattering (DLS) experiments show the change in size of the RMs upon encapsulation of the DNA molecules.

By using steady state and picosecond resolved fluorescence spectroscopy we have measured binding constants of EB with DNA molecules in buffer and in the RM. One major problem of using fluorescence technique to explore the nature of EB-binding to the DNA in RM is the massive interference of EB emission from the unbound EB in the RMs without DNA. Usually, ligand–DNA complex in nano-compartments (micelles, RM, vesicles, etc.) where there is a possibility of partitioning of the ligand to various microenvironments the background emission becomes unavoidable.<sup>11</sup> In our study we note that the relative concentration of the unbound EB in the RMs without DNA is up to 80% of the total RM in our sample. Exploration of EB binding with the DNA in such smaller number of RM would be a challenge to other standard experimental techniques including single molecule spectroscopy. We also show that even standard fluorescence techniques namely solvatochromic shift and time-resolved emission spectral (TRES) analyses are not good enough to address the nature of EB binding to DNA in RMs. To selectively address the nature of EB-binding with the DNA in the RM in

the presence of huge background emission of EB in the RM without DNA, picosecond resolved decay-associated spectral (DAS) technique has been successfully employed in this study. We confirm the presence of two types of binding modes of EB with the DNA in RMs, namely rigidly bound and loosely bound. The effect of concentration of AOT surfactant on the binding interaction has also been explored. Our time resolved fluorescence, CD, and DLS studies on the complexation of EB with two types of self-complementary synthetic oligonucleotides [(CGCAAATTTGCG)<sub>2</sub> and (GCGCGCGCGCGC)<sub>2</sub>] clearly demonstrate the nature of ligand binding and structure of small DNA molecules in the RM.

## EXPERIMENTAL DETAILS

DNA (from salmon testes) and bis(2-ethylhexyl)sulfosuccinate (AOT) were purchased from Sigma and used as received. Ethidium bromide (EB) and isooctane were from Molecular Probes and Spectrochem respectively. The purified (reverse phase cartridge) synthetic DNA oligonucleotides of 12 bases (dodecamer) with sequences CGCAAATTTGCG and GCGCGCGCGCGC were obtained from Gene Link. To reassociate the single strand DNA into self-complementary ds-DNA [(CGCAAATTTGCG)<sub>2</sub>, (oligo1), and (GCGCGCGCGCGC)<sub>2</sub>, (oligo2)] thermal annealing was performed as per the methodology prescribed by the vendor. The aqueous solutions of the oligonucleotides were dialyzed exhaustively against Millipore water prior to further use. The oligonucleotides of two different sequences were chosen because oligo1 is AT rich that binds EB differently than the GC rich oligo2. It has been noted that binding of EB to the oligonucleotides decreases with the increase in the ionic strength of the host solution. Aqueous sample solutions of genomic DNA were prepared in phosphate buffer (50 mM, pH 7). The procedure for making genomic DNA aqueous solution is similar to that described in Refs. 20 and 21. In the present study, the concentration of base pair of a DNA is considered as the overall concentration of the DNA. The nucleotide concentrations were determined by absorption spectroscopy using the average extinction coefficient per nucleotide of the DNA ( $6600\text{M}^{-1}\text{cm}^{-1}$  at 260 nm)<sup>20</sup> and found to be 5.0 mM (synthetic) and 21.45 mM (genomic). In other words, the base-pair concentrations in the stock solutions of synthetic and genomic DNA were measured to be 2.5 and 10.7 mM respectively. The DNA included RM with various  $w_0$  ([water]/[AOT]) was prepared by injecting known amount of aqueous EB and DNA into measured volume of AOT–isooctane solution.

Steady-state absorption and emission were measured with Shimadzu Model UV-2450 spectrophotometer and Jobin Yvon Model Fluoromax-3 fluorimeter respectively. CD spectra were taken in a Jasco-810 spectropolarimeter using a quartz cell of path-length 0.2 cm. Dynamic light scattering (DLS) measurements were done with Nano S Malvern instruments employing a 4 mW He-Ne laser ( $\lambda =$

632.8 nm) and equipped with a thermostated sample chamber. All the scattered photons were collected at 173° scattering angle at 298 K. The scattering intensity data were processed using the instrumental software to obtain the hydrodynamic diameter ( $d_H$ ) and the size distribution of the scatterer in each sample. The instrument measures the time-dependent fluctuation in intensity of light scattered from the particles in solution at a fixed scattering angle. Hydrodynamic diameters ( $d_H$ ) of the particles were estimated from the intensity auto correlation function of the time-dependent fluctuation in intensity.  $d_H$  is defined as,

$$d_H = kT/3\pi\eta D \quad (1)$$

where  $k$  is Boltzmann constant,  $T$  is absolute temperature,  $\eta$  is viscosity, and  $D$  is translational diffusion coefficient. In a typical size distribution graph from the DLS measurement  $x$ -axis shows a distribution of size classes in nanometer, while the  $y$ -axis shows the relative intensity of the scattered light. This is therefore known as an intensity distribution graph.

All fluorescence decays were taken by using picosecond-resolved time correlated single photon counting technique. The commercially available setup is a picosecond diode laser pumped time resolved fluorescence spectrophotometer from Edinburgh Instrument, UK. It has an instrument response function (IRF)  $\sim 80$  ps. The picosecond excitation pulse from Picoquant diode laser was used at 409 nm. A liquid scatterer was used to measure the FWHM of the IRF. Fluorescence from the sample was detected by a microchannel plate photo multiplier tube (Hamamatsu) after dispersion through a grating monochromator. For all decays, the polarizer in the emission side was adjusted to be at 54.7° (magic angle) with respect to the polarization axis of the excitation beam.

## Methods of Data Analysis

The observed fluorescence transients are fitted by using a nonlinear least square fitting procedure (software supplied by Edinburgh Instruments) to a function ( $X(t) = \int_0^t E(t') R(t-t') dt'$ ) comprising of convolution of the IRF ( $E(t)$ ) with a sum of exponentials ( $R(t) = A + \sum_{i=1}^N B_i e^{-t/\tau_i}$ ) with pre-exponential factors ( $B_i$ ), characteristic lifetimes ( $\tau_i$ ), and a background ( $A$ ). Relative concentration in a multiexponential decay is finally expressed as  $f_n = (\tau_n B_n / \sum_{i=1}^N B_i \tau_i) \times 100$ . The quality of the curve fitting was evaluated by reduced chi-square (0.90–1.09) and residual data. The purpose of the fitting is to obtain the decays in an analytic form suitable for further data analysis.

To construct TRES we follow the technique described in Refs. 22 and 23. As described earlier, the emission intensity decays are analyzed in terms of the multiexponential model,

$$I(\lambda, t) = \sum_{i=1}^N \alpha_i(\lambda) \exp[-t/\tau_i(\lambda)] \quad (2)$$

where  $\alpha_i(\lambda)$  are the pre-exponential factors, with  $\sum \alpha_i(\lambda) = 1.0$ . In this analysis we compute a new set of intensity

decays, which are normalized so that the time-integrated intensity at each wavelength is equal to the steady-state intensity at that wavelength. Considering  $F(\lambda)$  to be the steady-state emission spectrum, we calculate a set of  $H(\lambda)$  values using

$$H(\lambda) = \frac{F(\lambda)}{\int_0^\infty I(\lambda, t) dt} \quad (3)$$

which for multiexponential analysis becomes

$$H(\lambda) = \frac{F(\lambda)}{\sum_i \alpha_i(\lambda) \tau_i(\lambda)} \quad (4)$$

Then, the appropriately normalized intensity decay functions are given by

$$I'(\lambda, t) = H(\lambda) I(\lambda, t) = \sum_{i=1}^N \alpha'_i(\lambda) \exp[-t/\tau_i(\lambda)] \quad (5)$$

where  $\alpha'_i(\lambda) = H(\lambda) \alpha_i(\lambda)$ . The values of  $I'(\lambda, t)$  are used to calculate the intensity at any wavelength and time, and thus the TRES. The values of the emission maxima and spectral width are determined by nonlinear least-square fitting of the spectral shape of the TRES. The spectral shape is assumed to follow a lognormal line shape,<sup>22</sup>

$$I(\bar{\nu}) = I_0 \exp \left\{ - \left[ \ln 2 \left( \frac{\ln(\alpha + 1)}{b} \right)^2 \right] \right\} \quad (6)$$

with  $\alpha = \frac{2b(\bar{\nu} - \bar{\nu}_{\max})}{b}$  where  $I_0$  is amplitude,  $\bar{\nu}_{\max}$  is the wavenumber of the emission maximum and spectral width is given by  $\Gamma = \Delta[\sinh(b)/b]$ . The term  $b$  is an asymmetry parameter and Eq. (6) reduces to a Gaussian function for  $b = 0$ .

To ascertain two types of binding modes of EB with the DNA in the RM, we further follow time resolved area normalized emission spectral (TRANES) technique, which has been established in the literatures.<sup>24–26</sup> As described in the Refs. 24–26, TRANES is a model free modified version of TRES mentioned earlier. A useful feature of the method is that an isoemissive point in the spectra involves two emitting species, which are kinetically coupled either irreversibly or reversibly or not coupled at all. The selective information of the EB molecules with DNA in the RM comes from time resolved decay-associated spectra (DAS). As discussed in detail later, EB-DNA complex in buffer shows single exponential fluorescence decay with time constant of 22 ns. EB in RM without DNA reveals biexponential fluorescence decays with time constants of 1.5 and 4.5 ns. In the RM with DNA, EB shows three exponential fluorescence decays with two time constants (1.5 and 4.5 ns) similar to that in RM without DNA and third component varies from 11 to 22 ns depending on the detection wavelength. Our constructed DAS are the TRES of the longest components (11–22 ns) of the EB emission in the DNA-filled RM. However, the numerical fitting of the constructed DAS is performed by using sum of two lognormal functions [Eq. (6)] in the case of 100 and 200 mM AOT con-

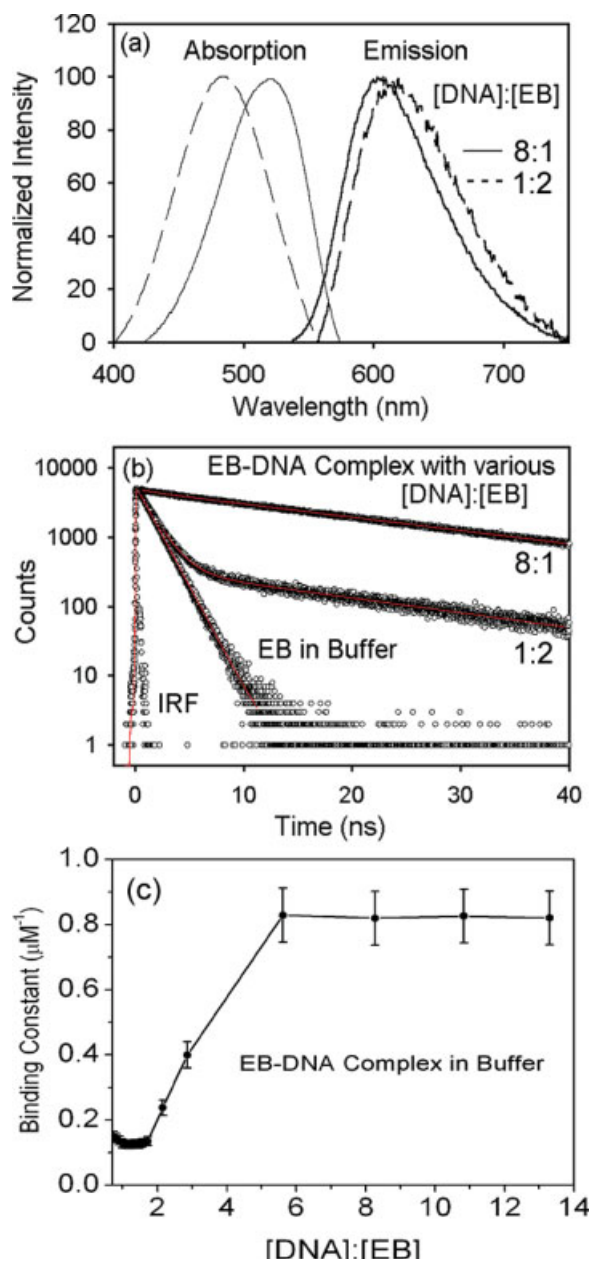


**FIGURE 1** (a) Steady state spectra of EB-DNA complex in buffer with various [DNA]:[EB]. (b) Fluorescence transients of various EB-DNA complexes in buffer. (c) Binding constants (10% standard error) of EB with DNA in buffer. Solid line is guide to the eye.

taining RMs. The goodness of the least square fitting of the constructed DAS as evidenced from reduced  $\chi^2$  reflects the existence of two kinds of population of the probe EB revealing two types of binding modes of the probe with DNA in the RM.

## RESULTS AND DISCUSSIONS

EB is a well-known fluorescent probe that readily intercalates into DNA double helix.<sup>27,28</sup> Figure 1a

shows absorption and emission spectra of EB-DNA (genomic) complex with various [DNA]:[EB]. Compared to bulk buffer, emission intensity and lifetime of EB increases nearly 11 times when it intercalates into the DNA double helix.<sup>29</sup> The observed Stokes shift decreases with the increase in [DNA]:[EB] ratio. In bulk buffer, the emission maximum of EB-DNA complex (605 nm at [DNA]:[EB] = 8:1) shows 25 nm

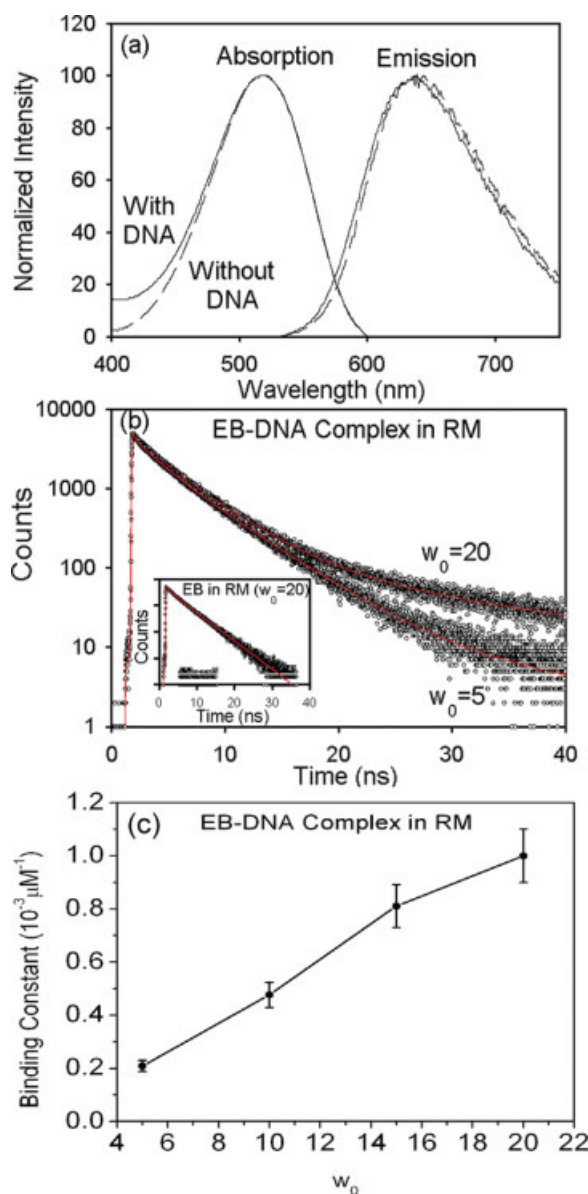


**FIGURE 2** (a) Steady state spectra of EB in the RM ( $w_0 = 20$ ) with and without the genomic DNA. (b) Picosecond resolved fluorescence transients of EB-DNA complex in RM with various sizes. Inset shows the transient of EB in RM ( $w_0 = 20$ ) without the genomic DNA for comparison. (c) Binding constants (10% standard error) of EB-DNA complex in RM with various  $w_0$  values. Solid line is guide to the eye. Here [DNA]:[EB] ratio is maintained at 8:1.

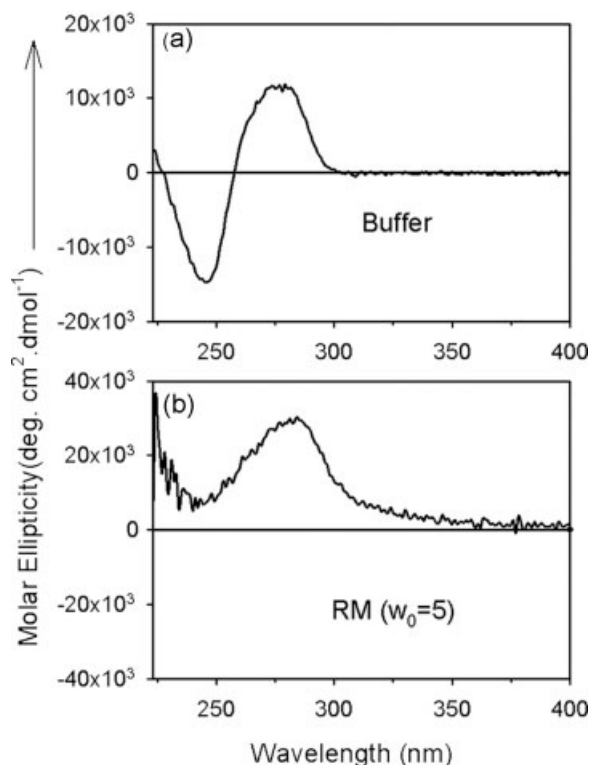


**FIGURE 3** CD spectra of the genomic DNA in (a) buffer and (b) the RM ( $w_0 = 5$ ) are shown.

blue shift when compared with free EB (630 nm). Picosecond resolved transients of EB in buffer and in EB-DNA complexes having different [DNA]:[EB] are shown in Figure 1b. EB in bulk buffer and completely complexed with DNA ([DNA]:[EB] = 8:1) show essentially single exponential fluorescence decays of time constants 1.5 and 22 ns respectively. In the transients, 1.5 ns component increases with the decrease in [DNA]:[EB] ratio, reflecting population of free EB in solution. By observing the relative percentage of 22 ns component in a fluorescence transient of a sample, which is the signature of the total population of EB bound to DNA molecules (EBDNA complex) and knowing the total concentrations of EB and DNA molecules, we calculate the binding constant ( $K$ ) of the ligand EB with the DNA in the sample by using following equation.

$$K = \frac{[\text{EBDNA}]}{([\text{EB}] - [\text{EBDNA}]) \times ([\text{DNA}] - [\text{EBDNA}])} \quad (7)$$

As shown in Figure 1c, the binding affinity of EB to the DNA at low [DNA]:[EB] ratio is relatively lower. It has been shown from other groups<sup>30,31</sup> that binding of EB with a genomic DNA can be categorized into two types, weak binding at lower [DNA]:[EB] ratio

(binding constant  $4 \times 10^4 M^{-1}$ ) and strong binding at higher [DNA]:[EB] ratio (binding constant  $100 \times 10^4 M^{-1}$ ). The measured strong binding constants at [DNA]:[EB] > 6:1 are consistent with the intercalative mode of binding of the ligand EB reported in the literatures.<sup>12,30–33</sup>

EB is extremely soluble in water (buffer) and completely insoluble in isoctane. Upon encapsulation into the RM, the cationic probes prefer to stay in the AOT–water interface.<sup>29</sup> The absorption (520 nm) and emission maxima (640 nm) of EB in the RM ([AOT] = 100 mM) in the presence and absence of DNA show similar features (Figure 2a). The fluorescence decay (at 640 nm) of EB in the RM ( $w_0 = 20$ ) (inset of Figure 2b) without DNA shows two time constants of 1.6 ns (10.14%) and 4.1 ns (87.65%). RMs containing EB-DNA show (Figure 2b) an additional longer decay component of 22 ns. This component indicates intercalation of EB in the DNA because the single-exponential decay of EB-DNA in buffer solution has a similar time constant of 22 ns (Figure 1b). The increase in the hydration level ( $w_0$ ) hence the size of

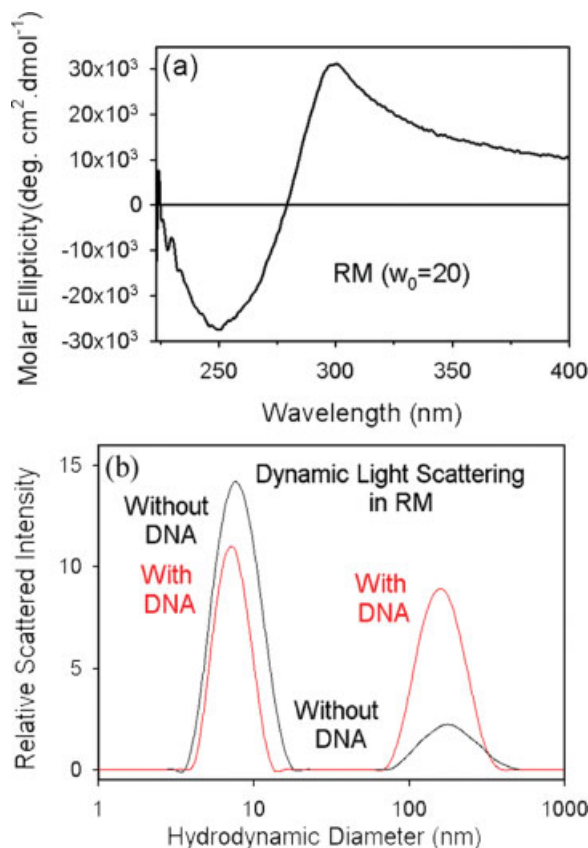


**FIGURE 4** (a) CD spectrum of the genomic DNA in the RM ( $w_0 = 20$ ) is shown. (b) DLS of RM ( $w_0 = 20$ , [AOT] = 100 mM) with and without the genomic DNA.

**Table I** DLS Data of RMs ( $w_0 = 20$ ) with and Without Genomic DNA

System	First peak		Second peak	
	$d_H$ (nm) <sup>a</sup>	Peak width (nm)	$d_H$ (nm) <sup>a</sup>	Peak width (nm)
RM ( $w_0 = 20$ ) without DNA				
100 mM AOT	7.8 (84.9)	2.2	118.9 (15.1)	36.8
200 mM AOT	9.1 (100)	3.2	—	—
300 mM AOT	9.8 (100)	4.0	—	—
400 mM AOT	8.8 (100)	2.7	—	—
RM ( $w_0 = 20$ ) with DNA (mM AOT)				
100 mM AOT	7.4 (46.4)	1.7	186.7 (53.6)	71.0
200 mM AOT	8.1 (35.6)	1.8	231.3 (64.4)	96.6
300 mM AOT	8.1 (60.8)	1.5	147.0 (39.2)	23.4
400 mM AOT	9.9 (100)	3.8	—	—

$d_H$  indicates hydrodynamic diameter of the RMs.

Peak width represents full width at half maximum of a particular scattering peak.

<sup>a</sup> Values in parenthesis indicate relative percentage of scattered light intensity.

the RM (radius of the water pool of the RM  $\approx 2 \times w_0$ <sup>34</sup>) expectedly affect DNA condensation by decreasing the curvature of the DNA.<sup>35</sup> In the fluorescence transients (Figure 2b), the increase of the pre-exponential values of time constant 22 ns (from 3 to 20%) with  $w_0$  (from  $w_0 = 5$  to 20) is clear evidence of the decrease of DNA curvature, which makes the stacking of EB into the DNA relatively more stable. Our studies of the EB-DNA complex in the RM with various  $w_0$  also reveal enhance efficacy of intercalation in the nanospace upon increase in degree of hydration or size of the RM (Figure 2c). Recently, steady-state quenching studies on EB-DNA complex in a neutral RM revealed similar effect of perturbation of intercalation and concluded to be due to bending of the DNA in the nanospace.<sup>4</sup> The decrease in the EB affinity for the DNA in the RM ( $0.2\text{--}0.8 \times 10^3 M^{-1}$ ) when compared with that in buffer solution ( $80 \times 10^5 M^{-1}$ ) clearly indicates that the stacking of the probe EB into the DNA in the RM is perturbed when compared with the efficient stacking (intercalation) of the probe in the DNA in bulk buffer.

CD spectra of the genomic DNA in the RM with various  $w_0$  values are shown in Figures 3 and 4. The structural studies indeed show the change in the form of the DNA in the RM when compared with that in buffer (Figure 3a), which is the characteristic of B form DNA.<sup>18,19</sup> The CD spectrum of the DNA in RM at  $w_0 = 5$  (Figure 3b) undergoes a sharp change, characteristic of the B  $\rightarrow$   $\psi$ -form transition.<sup>19</sup> The transition is associated with the condensation of the DNA in the nanospace. In contrast to the CD spectrum of the DNA in the buffer solution, in the RMs with  $w_0 = 10, 15,$  and 20, the spectra show (spectrum of the DNA in RM at  $w_0 = 20$  is shown in Figure 4a) fol-

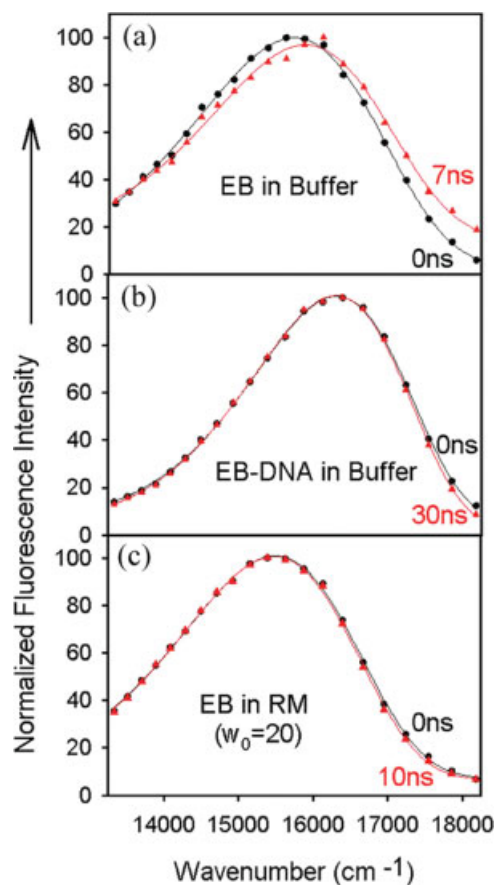


**FIGURE 5** TRES of (a) EB in buffer, (b) EB-DNA (genomic) in buffer, (c) EB in RM ( $w_0 = 20$ ) respectively. Note that the scattered plots are the experimental data and line plots are the lognormal fitting data. Here, [DNA]:[EB] ratio is maintained at 8:1.

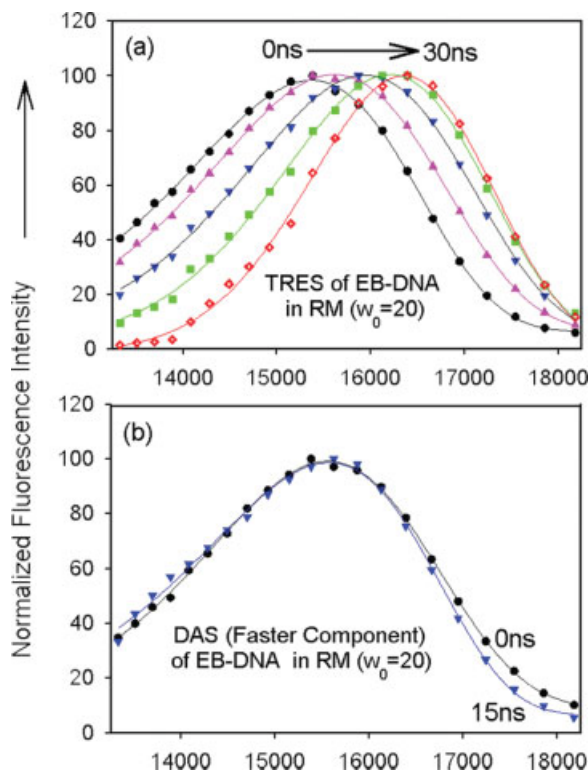


**FIGURE 6** (a) TRES. (b) DAS (faster component) of EB-DNA (genomic) complex in RM ( $w_0 = 20$ , [AOT] = 100 mM) are shown. Note that the scattered plots are the experimental data and line plots are the lognormal fitting data. Here, [DNA]:[EB] ratio is maintained at 8:1.

lowing common features: (i) an increase in both positive and negative molar ellipticities, (ii) a shift in crossover point, (iii) a negative absorption at around 260 nm, and (iv) an appreciable absorption at longer wavelengths. The spectral characteristics are consistent with the formation of aggregated form of the genomic DNA.<sup>18,36</sup>

The intensity distribution of the scattered light from DLS measurement on the RM ( $w_0 = 20$ , [AOT] = 100 mM) in the presence and absence of the genomic DNA is shown in Figure 4b. The expected hydrodynamic diameter of the RMs at this hydration level is  $\sim 9$  nm.<sup>34</sup> From DLS studies (Table I), existence of larger-sized RMs are evidenced. It was also observed that the concentration of the larger-sized RM increases upon addition of DNA to the RM solutions at 100 mM AOT. DLS studies on the RMs (100 mM AOT concentration) with DNA at various  $w_0$  (5–20) also show (data not shown) the presence of larger particle size ( $\sim 150$  nm). Previously, it has been shown<sup>18</sup> that the possibility of residence of DNA in the larger RMs is relatively higher. Thus, any heterogeneity in the binding efficacy of EB with the DNA

in the RM is expected to be because of two different kinds of population of the condensed DNA in the RM. However, our studies confirmed (see later) the heterogeneity of EB binding sites of the DNA even in monodispersed RM solutions.

TRES constructed from the transients of EB in buffer (Figure 5a), EB-DNA (genomic) in buffer (Figure 5b), and EB in RM ( $w_0 = 20$ ) (Figure 5c) do not show significant spectral change. The TRES of EB-DNA complex in the RM ( $w_0 = 20$ ) shows an apparent spectral blue shift ( $\Delta\nu = 1028 \text{ cm}^{-1}$ , Figure 6a). The shift is due to the presence of faster time constants (1.5 and 4.1 ns) in the red side and relatively longer one (22 ns) in the blue side of the emission spectrum. DAS for faster and slower components of the TRES of the probe give information of EB in the RMs ( $w_0 = 20$ ) without (Figure 6b) and with (Figure 7a) the DNA respectively. The DAS for the faster decay components, which is a signature of EB

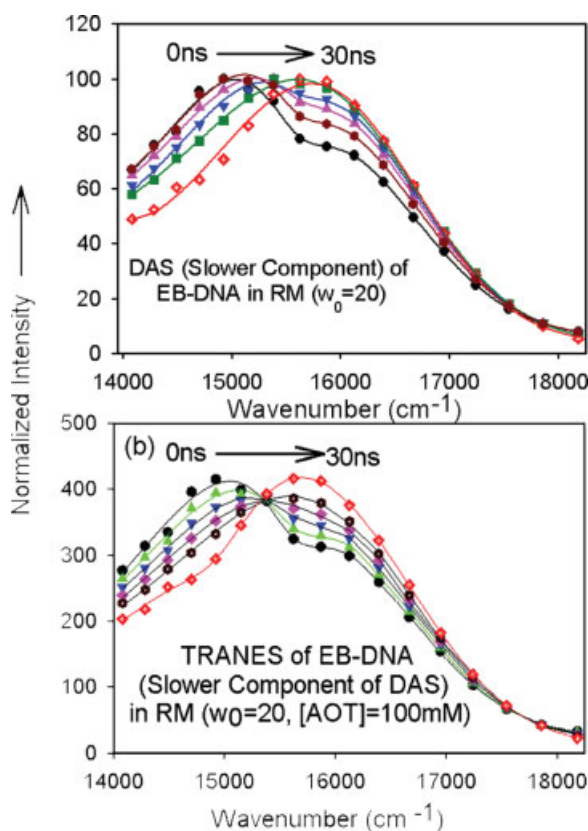


**FIGURE 7** (a) DAS (slower component). (b) Time-resolved area normalized DAS (TRANES, slower component) of EB-DNA (genomic) complex in 100 mM AOT/isooctane RM ( $w_0 = 20$ ). Note that the scattered plots are the experimental data and line plots are the double-lognormal fitting data. Here, [DNA]:[EB] ratio is maintained at 8:1.

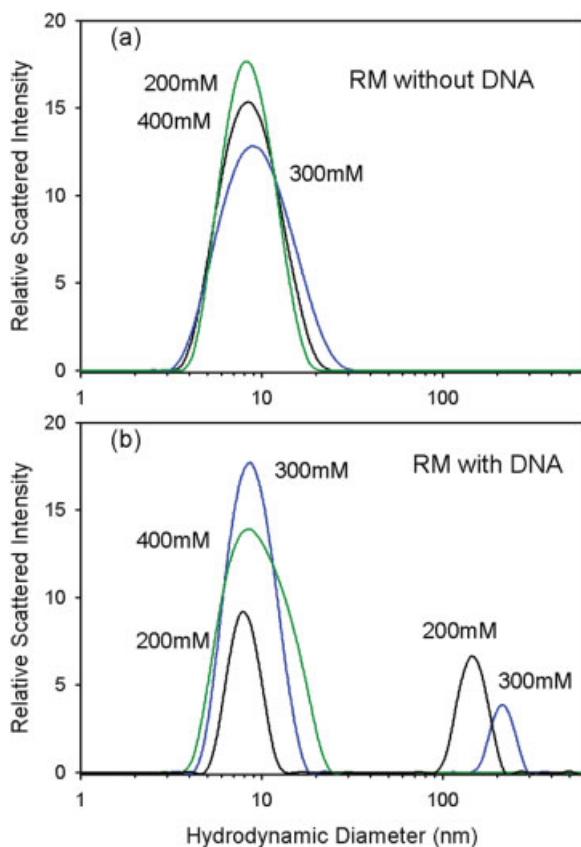


**FIGURE 8** DLS data of RM (a) without and (b) with the genomic DNA at various AOT concentrations.

in the RMs without DNA, do not change with time (Figure 6b). The DAS for the slower decay components reflecting dynamical events of EB in the RMs with the DNA show (Figure 7a) a unique feature, indicating the presence of two types of DNA-bound ligands in the nanospace. Numerical fit (solid line) of the spectra by two lognormal spectral functions (two peaks) shows gradual decrease of one of the peaks at  $14,925\text{ cm}^{-1}$  and corresponding rise at  $15,886\text{ cm}^{-1}$ . The blue shifted and red shifted peaks in the DAS are consistent with the EB emission in free and DNA bound state respectively (Figure 1a). In Figure 7a, the blue-shifted peak at  $15,886\text{ cm}^{-1}$  and red-shifted peak at  $14,925\text{ cm}^{-1}$  of EB are assigned as strong interaction (intercalative-type) and binding to a partially *perturbed* site of the DNA respectively. To ascertain the possible coexistence of two species in the nanospace, we further used TRANES technique. An isoemissive point at  $15,384\text{ cm}^{-1}$  is clearly evident in the TRANES (Figure 7b).

As evidenced in Figure 4b, two kinds of reverse micellar population ( $\sim 9$  and  $\sim 150$  nm) might be responsible for the binding heterogeneity of EB to DNA in the RM ( $w_0 = 20$ ,  $100\text{ mM}$  [AOT]). Our

DLS studies on the RM ( $w_0 = 20$ ) show that the population of larger-sized RM ( $\sim 150$  nm) depends on the concentration of the AOT surfactant in the reverse micellar solution (Figure 8). The RMs without DNA show the existence of larger particles at  $100\text{ mM}$  AOT concentration (Figure 4b and Table I). In contrast, the RMs with DNA continue to show the presence of larger-sized particles up to  $300\text{ mM}$  AOT

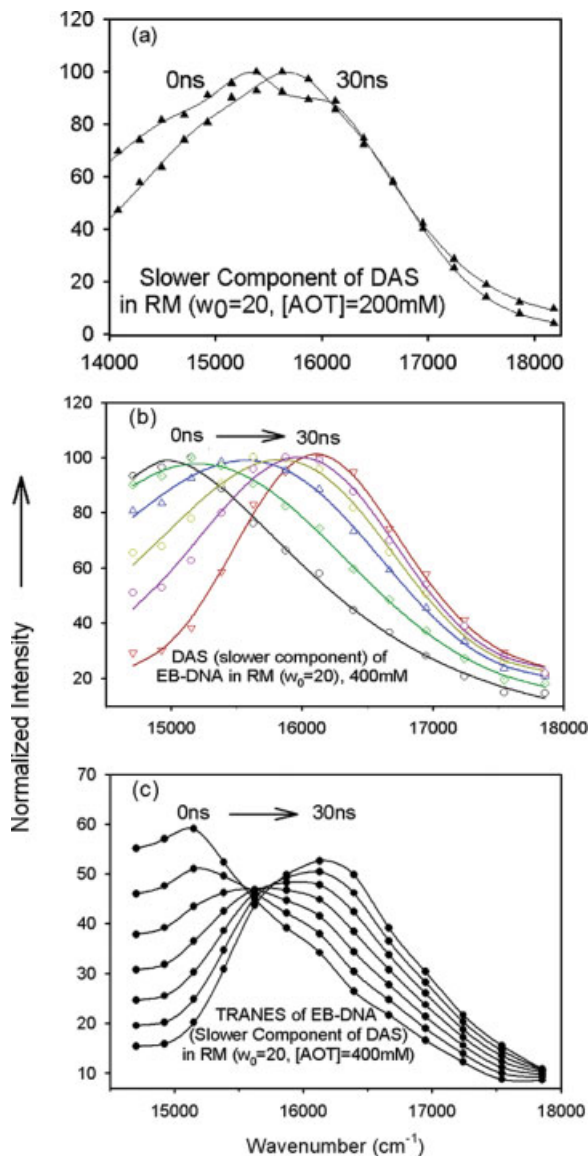


**FIGURE 9** DAS of EB-DNA complex in the RM at  $w_0 = 20$  (a) with  $200\text{ mM}$  AOT (b) with  $400\text{ mM}$  AOT concentrations. Note that the scattered plots are the experimental data and line plots are the (a) double and (b) single lognormal fitting data. (c) TRANES of the slower component of EB-DNA complex in RM at  $400\text{ mM}$  AOT concentration. Solid lines are guides to the eye. Here, [DNA]:[EB] ratio is maintained at 8:1.

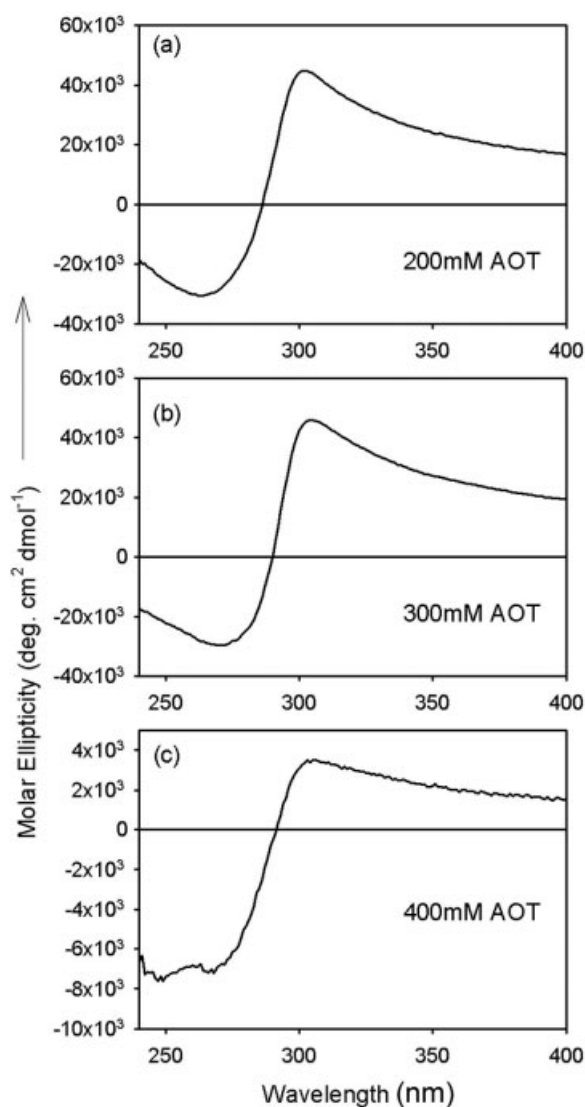


**FIGURE 10** CD spectra of the genomic DNA in the RMs ( $w_0 = 20$ ) with various AOT concentrations.

concentration (Figure 8b and Table I). We also observed that in the presence of the DNA, the relative population of larger-sized RMs increases with the concentration of AOT up to 200 mM and then starts decreasing to a vanishingly small value at 400 mM [AOT] (Figure 8b and Table I). Thus, the studies of EB–DNA complex in the RM with 400 mM AOT concentration give us opportunity to investigate the nature of EB-binding to the DNA in the nanospace without any structural heterogeneity of the RM.

DAS and TRANES spectra of the probe EB with the genomic DNA in the RM with various AOT concentrations are shown in Figure 9. The DAS spectra for the slower time constants of EB–DNA complexes in the RMs ( $w_0 = 20$ ) with 200 mM AOT concentra-

tion is shown in Figure 9a. The temporal nature of the DAS shows similar behavior to that of RM with 100 mM AOT giving loosely and strongly bound EB at 15,384 and 15,870 cm<sup>-1</sup> respectively. In contrast to 100 mM AOT–RM, the emission peak for the loosely bound EB (15,384 cm<sup>-1</sup>) is blue shifted, indicating relative reclamation of relaxed state of the DNA in the 200 mM AOT–RM. The less-condensed relaxed state of the DNA in the 200 mM AOT RM could be due to the incorporation of the DNA molecules in the larger-sized water pools of the RM.<sup>18</sup>

In the RM with 400 mM AOT concentration, where the distribution of the reverse micellar size is essentially monodispersed, the slower component DAS (Figure 9b) shows two binding modes of the probe EB with the DNA reflecting loosely and strongly bound EB at 14,969 and 16,105 cm<sup>-1</sup> respectively. The positions of the peaks at earlier and longer times are similar to those in 100 mM AOT RM. The constructed TRANES (Figure 9c) also show an isoemissive point at 15,625 cm<sup>-1</sup>, reflecting the presence of two emissive species in the RM. Our studies clearly demonstrate that two types of binding

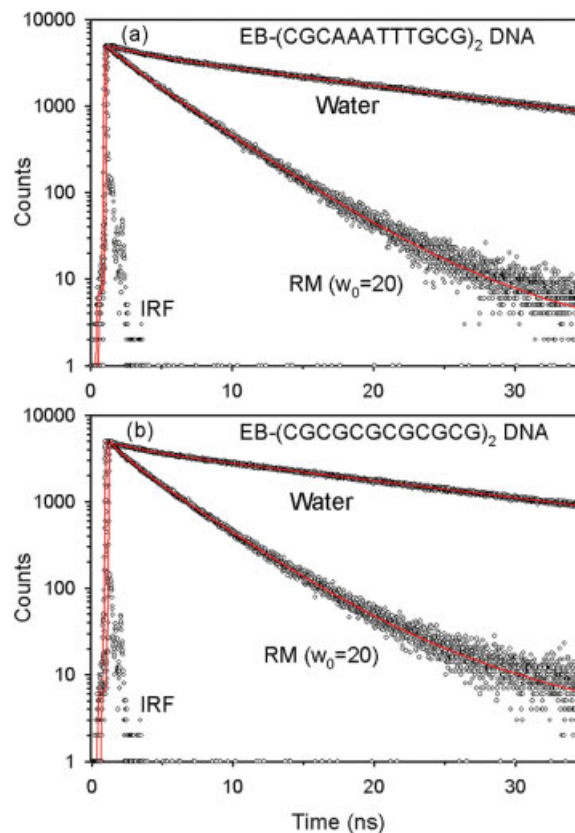


**FIGURE 11** Picosecond resolved fluorescence transients of EB with various oligonucleotides in water and in the RM ( $w_0 = 20$ ) are shown.

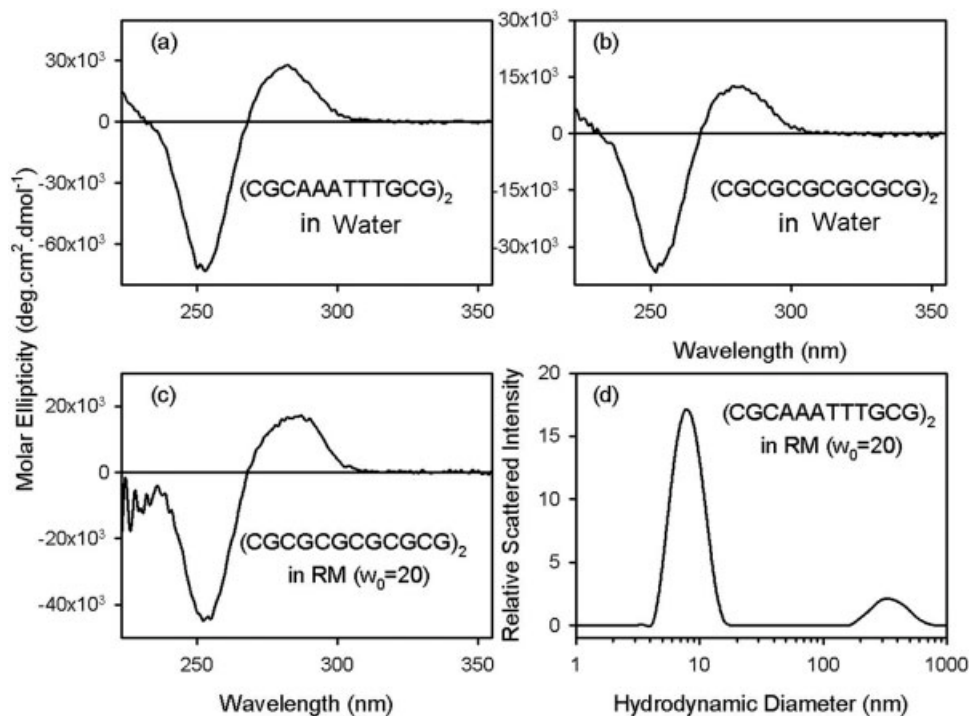


**FIGURE 12** CD spectra of the oligonucleotides in water (a and b) and in the RM (c) are shown. Note that the CD spectrum of the (CGCAAATTTGCG)<sub>2</sub> is found to be similar to that of the (CGCGCGCGCGCG)<sub>2</sub> and hence not shown. The DLS data of the RM with (CGCAAATTTGCG)<sub>2</sub> is shown in (d). The DLS data of the (CGCGCGCGCGCG)<sub>2</sub> is found to be similar to that of the (CGCAAATTTGCG)<sub>2</sub> and hence not shown.

modes are possible in the condensed DNA entrapped in the RMs with uniform size distribution and hence can be assigned as the nature of the ligand binding of the condensed DNA. The structural changes of the DNA in the RM are evidenced from CD spectroscopic studies as shown in Figure 10. The DNA structures in the RM up to 300 mM AOT are similar in nature, which is consistent with the aggregated form of the DNA in the nanospace.<sup>18,36</sup> In 400 mM AOT RM (Figure 10c), the DNA structure is somewhat different than those in 100–300 mM AOT RMs with  $w_0 = 20$ , particularly increased absorption in the negative direction ( $\sim 250$  nm) relative to that in the positive direction ( $\sim 300$  nm). However, the overall feature of the CD spectrum (Figure 10c) is also consistent with the aggregated form of the DNA.

We also investigate the effect of reverse micellar environments on the secondary structure of short DNA oligonucleotides having total length ( $\sim 4.1$  nm) lesser than the diameter of the reverse micellar water pool at  $w_0 = 20$  ( $\sim 9$  nm). We have studied the complexation of EB with oligo1 and oligo2. The fluorescence transients of the EB-oligonucleotide complexes in water and in the RM (100 mM AOT and  $w_0 = 20$ )

are shown in Figure 11. The binding constants of EB with oligo1 and oligo2 in water are  $47 \times 10^4$  and  $101 \times 10^4 M^{-1}$  respectively. Temporal EB-fluorescence transients show significant decrease in the ligand binding affinity (binding constants are  $5.0 \times 10^2$  and  $16.6 \times 10^2 M^{-1}$  for oligo1 and oligo2 respectively) of EB to the oligonucleotides in the RM. The decrease in the EB binding to the oligonucleotides in the RM could be due to the significant affinity of the probe towards the interface of the RM.<sup>11</sup> The constructed DAS (data not shown) of the slower (22 ns) components are featureless as the fluorescence transients across the emission spectrum of EB-oligonucleotide complexes in the RM overlap with each other. These observations rule out the possibility of multiple binding sites of the probe EB with the oligonucleotides in the RM. Structural studies (Figures 12a–12c) on the oligonucleotides in buffer and in the RM show insignificant perturbation of the B-form upon encapsulation of the synthetic DNA molecules in the RM. Our observations are consistent with a recent report of insignificant structural perturbation of (GATGAGAGTTAGTGATGAGTG)<sub>2</sub> oligonucleotide in AOT RM.<sup>37</sup> The structures of the RMs

with oligonucleotides as evidenced from DLS studies (Figure 12d) are similar to that of the RMs with the genomic DNA (Figure 4b). These observations clearly indicate that the environments of the RM ( $w_0 = 20$ ) do not have any effect on the secondary structure of the DNA.

## CONCLUSION

Our studies on the complexation of a ligand EB to a genomic DNA (from salmon testes) in an anionic (AOT) RM shows significant alteration of interaction (intercalation) of the ligand to the DNA molecules in the nanospace. CD spectroscopy reveals condensed form of the DNA in the RM. From picosecond resolved DAS of EB-DNA complex in the RM, selective information on the dynamics of EB-binding to the condensed DNA is obtained. As evidenced from our work, ordinary TRES of the complex are incapable of providing information about two types of EB binding (namely strong and loose) in the condensed DNA inside the RM because of the presence of huge background EB emission from the RMs without DNA. Analysis of time resolved DAS of EB in RMs with the genomic DNA selectively explores the nature of ligand binding of the DNA in the nanospace. The studies indicate a temporal decay in the population of loosely bound photoexcited EB ( $\sim 15,000 \text{ cm}^{-1}$ ) and corresponding rise in the strongly bound EB ( $\sim 16,000 \text{ cm}^{-1}$ ) in the RM. The observation clearly shows the presence of two types of EB-binding modes with the genomic DNA in the RM. The picosecond resolved DAS and TRANES studies of the DNA in RMs with various AOT concentrations indicate that condensed DNA even in monodispersed RMs offers two kinds of binding modes to the ligand EB molecules. The studies of the EB-oligonucleotides complexes in the RM reveal insignificant environmental effect on the secondary structure and EB-binding of the DNA molecules. Our observations clearly demonstrate that the alteration of ligand binding mode of the genomic DNA compared to that in the buffer solution is *solely* due to the condensation of the DNA in the nanospace of the RMs. These experimental methodologies will be useful for further studies into the mechanism of DNA condensation.

RS thanks UGC for the fellowship.

## REFERENCES

- Dervan, P. B. *Bioorg Med Chem* 2001, 9, 2215–2235.
- Bloomfield, V. A. *Biopolymers* 1991, 31, 1471–1481.
- Bloomfield, V. A. *Curr Opin Struct Biol* 1996, 6, 334–341.
- Budker, V. G.; Slattum, P. M.; Monahan, S. D.; Wolf, J. A. *Biophys J* 2002, 82, 1570–1579.
- Strzelecka, T. E.; Rill, R. L. *Biopolymers* 1990, 30, 803–814.
- Strzelecka, T. E.; Rill, R. L. *Biopolymers* 1990, 30, 57–71.
- Battistel, E.; Imre, E. V.; Luisi, P. L. *Controlled Release of Drugs: Polymers and Aggregate Systems*; Wiley-VCH Verlag: Weinheim, Germany, 1989.
- Imre, V. E.; Luisi, P. L. *Biochem Biophys Res Commun* 1982, 107, 538–545.
- Luisi, P. L.; Magid, L. J. *Crit Rev Biochem* 1986, 20, 409–474.
- Park, L. C.; Maruyama, T.; Goto, M. *Analyst* 2003, 128, 161–165.
- Shaw, A. K.; Sarkar, R.; Pal, S. K. *Chem Phys Lett* 2005, 408, 366–370.
- LePecq, J.-B.; Paoletti, C. *J Mol Biol* 1967, 27, 87–106.
- Dalgleish, D. G.; Peacocke, A. R. *Biopolymers* 1971, 10, 1853–1863.
- Erard, M.; Das, G. C.; de Murcia, G.; Mazen, A.; Pouyet, J.; Champagne, M.; Daune, M. *Nucleic Acids Res* 1979, 6, 3231–3253.
- Angerer, L. M.; Georghiou, S.; Moudrianakis, E. N. *Biochemistry* 1974, 13, 1075–1082.
- Lurquin, P. F.; Seligy, V. L. *Biochem Biophys Res Commun* 1972, 46, 1399–1404.
- Winzeler, E. A.; Small, E. W. *Biochemistry* 1991, 30, 5304–5313.
- Pietrini, A. V.; Luisi, P. L. *Biochim Biophys Acta* 2002, 1562, 57–62.
- Kankia, B. I.; Buckin, V.; Bloomfield, V. A. *Nucleic Acids Res* 2001, 29, 2795–2801.
- Cosa, G.; Focsaneanu, K.-S.; McLean, R. N.; McNamee, J. P.; Scaiano, J. C. *Photochem Photobiol* 2001, 73, 585–599.
- Gallagher, S. R. In *Current Protocols in Molecular Biology*; Ausubel, F. M.; Brent, R.; Kingston, K. E.; Moore, D. D.; Seidman, J. G.; Smith, J. A.; Struhl, K., Eds.; Greene and Wiley-Interscience: New York, 1994.
- Hornig, M. L.; Gardecki, J. A.; Papazyan, A.; Maroncelli, M. *J Phys Chem* 1995, 99, 17311–17337.
- Lakowicz, J. R. *Principles of Fluorescence Spectroscopy*; Kluwer Academic and Plenum: New York, 1999.
- Periasamy, N.; Koti, A. S. R. *Proc Indian Natl Sci Acad Part A: Phys Sci* 2003, 69, 41–48.
- Koti, A. S. R.; Krishna, M. M. G.; Periasamy, N. *J Phys Chem A* 2001, 105, 1767–1771.
- Koti, A. S. R.; Periasamy, N. *Proc Indian Natl Sci Acad: Chem Sci* 2001, 113, 157–163.
- Fiebig, T.; Wan, C.; Kelley, S. O.; Barton, J. K.; Zewail, A. H. *Proc Natl Acad Sci USA* 1999, 96, 1187–1192.
- Millar, D. P.; Robbins, R. J.; Zewail, A. H. *J Chem Phys* 1982, 76, 2080–2094.

29. Pal, S. K.; Mandal, D.; Bhattacharyya, K. *J Phys Chem B* 1998, 102, 11017–11023.
30. Vardevanyan, P. O.; Antonyan, A. P.; Parsadanyan, M. A.; Davtyan, H. G.; Karapetyan, A. T. *Exp Mol Med* 2003, 35, 527–533.
31. McMurray, C. T.; van Holde, K. E. *Biochemistry* 1991, 30, 5631–5643.
32. McMurray, C. T.; Small, E. W.; van Holde, K. E. *Biochemistry* 1991, 30, 5644–5652.
33. Alonso, A.; Almendral, M. J.; Curto, Y.; Criado, J. J.; Rodriguez, E.; Manzano, J. L. *Anal Biochem* 2006, 355, 157–164.
34. De, T. K.; Maitra, A. *Adv Colloid Interface Sci* 1995, 59, 95–193.
35. Conwell, C. C.; Vilfan, I. D.; Hud, N. V. *Proc Natl Acad Sci USA* 2003, 100, 9296–9301.
36. Thomas, T. J.; Thomas, T. *Nucleic Acids Res* 1989, 17, 3795–3810.
37. Evans, S. E.; Mon, S.; Singh, R.; Ryzhkov, L. R.; Szalai, V. A. *Inorg Chem* 2006, 45, 3124–3132.

*Reviewing Editor: Sarah Woodson*